Quaternary Ag/AgCl/TiO$_2$/MWCNTs nanocomposite: an efficient visible-light-driven plasmonic photocatalyst for degradation of 2,4-dichlorophenol

Pouya Seirafi[a], Azadeh Ebrahimian Pirbazari[a,b,*], Mohammad Ali Aroon[a]

[a]Caspian Faculty of Engineering, College of Engineering, University of Tehran, P.O. Box 43841-119, Rezvanshahr 43861-56387, Iran, emails: pouya.seirafi2006@gmail.com (P. Seirafi), maaroon@ut.ac.ir (M.A. Aroon)
[b]Fouman Faculty of Engineering, College of Engineering, University of Tehran, P.O. Box 43515-1155, Fouman 43516-66456, Iran, Tel. +981334734927; Fax: +981334737228; email: aebrahimian@ut.ac.ir (A.E. Pirbazari)

ABSTRACT

In this research, we developed a facile method to synthesize quaternary plasmonic photocatalysts Ag/AgCl/TiO$_2$/MWCNTs with a high photocatalytic performance for degradation of 2,4-dichlorophenol (2,4-DCP) under visible light. The prepared samples were characterized by different analyses such as X-ray diffraction, scanning electron microscopy, energy dispersive X-ray, ultraviolet-visible diffuse reflectance spectroscopy, Fourier transform infrared spectroscopy, N$_2$ physisorption, and transmission electron microscopy. The prepared samples exhibited highly visible-light photocatalytic efficiency for degradation of 2,4-DCP in aqueous solution. In the presence of pure TiO$_2$ and quaternary Ag/AgCl/TiO$_2$/MWCNTs nanocomposite, we obtained 40% and almost 100% degradations of 2,4-DCP under visible light after 180 min irradiation, respectively. The excellent visible light photocatalytic activity of Ag/AgCl/TiO$_2$/MWCNTs samples can be attributed to the surface plasmon resonance effect of Ag nanoparticles anchored on AgCl particles and adsorption ability of MWCNTs.

Keywords: Ag/AgCl; Plasmonic photocatalysts; MWCNTs; Degradation; 2,4-DCP

1. Introduction

Preparation of efficient semiconductor-based photocatalysts using visible light for environmental application and energy conversion is a great challenge [1–4]. Many efforts by narrowing the band gap of TiO$_2$, including element doping and oxygen deficiency, have been dedicated to enhancing visible-light absorption [2,5,6]. Unfortunately, TiO$_2$ doping with impurity species often leads to the impaired photocatalytic efficiency of TiO$_2$ because the doped atoms accelerate carrier recombination rate [2,7]. Modification of TiO$_2$ by noble metals such as Au and Ag has been the subject of intense research because of its significant positive role in the photocatalytic efficiency [8–10]. Nobel metals such as Ag and Au nanoparticles display very interesting optical properties due to the excitation of resonant collective oscillations of the conduction electrons by electromagnetic radiation: the localized surface plasmon resonance (LSPR) [11–13]. LSPR can noticeably increase the visible-light absorption and thus enhance the plasmonic photocatalysts yield with high efficiency under visible light for environmental applications. Silver halide materials (AgX, X: Cl, Br, and I) show good stability compared with the traditional noble metal/semiconductor plasmonic systems because of remaining unchanged after decomposition into Ag^0 species under irradiation [14]. Moreover, they are among the most promising plasmonic photocatalysts [15]. Recently, many attempts have been made to prepare AgCl-based TiO$_2$ nanomaterials for efficient degradation of organic and inorganic pollutants [16–28]. AgCl as a photosensitive material is used for inactivation of bacteria and degradation of organic pollutants [29]. In AgCl-based TiO$_2$ photocatalyst, the photogenerated electrons generated under light irradiation would combine with a silver cation (Ag$^+$) to produce metallic silver (Ag^0). Thus, the formed Ag clusters could alter the photoactive

* Corresponding author.

range of AgCl well into the visible region [20,29–31]. Also, it has been evidenced that the addition of cosorbent carbon materials can enhance the photocatalytic efficiency of TiO_2 [32–34]. Since their discovery, multi-walled carbon nanotubes (MWCNTs) with one-dimensional and hollow structure have received more attention for environmental purification because of their outstanding structural characters such as mechanical strength [35], excellent thermal conductivity, unique electronic properties [36], and thermal stability [37]. The preparation of new composite containing MWCNTs and TiO_2 depends on many factors such as excellent conductance and high adsorption capacity of MWCNTs, which act as TiO_2 support [38,39]. A similar literature has shown that the activities of the TiO_2 increase due to the abilities of MWCNTs to decrease TiO_2 crystalline grain and particle sizes [40]. Also, these activities increase the activity of the particles because of the connection between MWCNTs and TiO_2 reduces the recombination of electron and hole (h^+/e^-) [41].

To combine the synergetic properties of the MWCNTs and plasmas, the $Ag/AgCl/TiO_2/MWCNTs$ nanocomposites as new visible-light-driven plasmonic photocatalysts were prepared through a simple synthesis method by direct reaction of HCl and $AgNO_3$. The prepared $Ag/AgCl/TiO_2/MWCNTs$ nanocomposites were characterized by several techniques including X-ray diffraction (XRD), Fourier transform infrared spectroscopy (FTIR), scanning electron microscopy (SEM)/energy dispersive X-ray (EDX), transmission electron microscopy (TEM), N_2 physisorption, and ultraviolet-visible diffuse reflectance spectroscopy (DRS). The photocatalytic activity of the nanocomposites was investigated in terms of the photocatalytic degradation of 2,4-dichlorophenol (2,4-DCP) as a model of an organic pollutant under visible light ($\lambda > 400$ nm). Chlorophenols are toxic chemicals used in many industrial applications such as petrochemicals, pesticide, dye intermediates, and dyes [42]. 2,4-DCP is a chemical precursor commonly used for the production of herbicide 2,4-dichlorophenoxyacetic acid (2,4-D) [43]. However, 2,4-DCP also has some disadvantageous such as causing some pathological symptoms and altering human endocrine systems. The exposure mode of 2,4-DCP is through the skin and gastrointestinal tract. In recent years, chlorophenols persistence and bioaccumulation both in animals and in humans have raised concerns about these compounds [44–46]. Hence, searching to find novel and efficient ways to minimize the harm of organic pollutants such as chlorophenols in the environment is of high importance. In the present research, we report the first work on the preparation of quaternary $Ag/AgCl/TiO_2/MWCNTs$ nanocomposites through a simple sol–gel method. The outstanding properties associated the nanocomposites suggested that they can be used as a novel plasmonic visible-light-driven catalyst for given applications in photocatalysis.

2. Experimental

2.1. Materials and reagents

To synthesize the photocatalyst, silver nitrate ($AgNO_3$, 99.9%) was purchased from Merck (Germany) (No. 101510). Titanium isopropoxide (TIP) was supplied from Merck (No. 821895), ethanol was supplied from Merck (No. 818760), and deionized water and MWCNTs functionalized by carboxylic groups were provided by Neutrino Corporation, Iran. The average diameter and length of the MWCNTs were 10–20 nm and 0.5–2 μm, respectively. High-purity 98% 2,4-DCP (Merck No. 803774) was used as a probe molecule for photocatalytic tests.

2.2. Preparation of Ag/AgCl/TiO₂/MWCNTs nanocomposite

$Ag/AgCl/TiO_2/MWCNTs$ nanocomposites were prepared by a simple and modified sol–gel procedure. An appropriate amount of $AgNO_3$ (Table 1), 10 mL TIP, and 30 mL ethanol was stirred for 2 h (solution A). Then, solution B, 20 mL ethanol, 5 mL deionized water and 2 mL hydrochloric acid and an amount of MWCNTs (Table 1) was added into the solution A and stirred for 12 h at room temperature. The sol formed after 12 h of stirring followed by aging at room temperature for 24 h and evaporated at 80°C for 8 h. Finally, the dried powder was calcined at 450°C under air for 2 h to get an $Ag/AgCl/TiO_2/MWCNTs$ sample. For the sake of comparison, four $Ag/AgCl/TiO_2/MWCNTs$ samples containing different amounts of MWCNTs, pure TiO_2, $Ag/AgCl/TiO_2$, and $MWCNTs/TiO_2$ samples were synthesized by the same route. From now on, the prepared samples are labelled according to Table 1.

2.3. Characterization

FTIR analysis was applied to determine the surface, functional groups, using FTIR spectroscopy (FTIR-2000, Bruker), where the spectra were recorded from 4,000 to 400 cm^{-1}. The

Table 1
Nomenclatures of the prepared samples

Samples	Materials	Nomenclatures
TiO_2	10 mL TIP	TiO_2
$MWCNTs/TiO_2$	0.92 g[a] MWCNTs + 10 mL TIP	$MWCNTs/TiO_2$
$Ag/AgCl/TiO_2$	0.1 g $AgNO_3$ + 10 mL TIP	$Ag/AgCl/TiO_2$
$Ag/AgCl/TiO_2/MWCNTs$	0.050 g MWCNTs + 0.1 g $AgNO_3$ + 10 mL TIP	$Ag/AgCl/TiO_2/MWCNTs$ (2.00)[b]
$Ag/AgCl/TiO_2/MWCNTs$	0.066 g MWCNTs + 0.1 g $AgNO_3$ + 10 mL TIP	$Ag/AgCl/TiO_2/MWCNTs$ (3.00)
$Ag/AgCl/TiO_2/MWCNTs$	0.083 g MWCNTs + 0.1 g $AgNO_3$ + 10 mL TIP	$Ag/AgCl/TiO_2/MWCNTs$ (4.00)
$Ag/AgCl/TiO_2/MWCNTs$	0.166 g MWCNTs + 0.1 g $AgNO_3$ + 10 mL TIP	$Ag/AgCl/TiO_2/MWCNTs$ (6.00)

[a]The average amount of MWCNTs that used for synthesis of $Ag/AgCl/TiO_2/MWCNTs$ samples.
[b]The number in parenthesis is the theoretical weight percentage of MWCNTs.

XRD patterns were recorded using a Siemens D5000 (Germany) apparatus. The diffractograms were recorded in the 2θ range of 20°–80° using an X-ray diffractometer equipped with Cu K$_\alpha$ radiation as the X-ray source. The morphology of the prepared samples was characterized using SEM (Vegall-Tescan Company, Czech Republic) equipped with an EDX. The diffuse reflectance UV–Vis spectra (DRS) of the samples were recorded using an Ava Spec-2048TEC spectrometer.

2.4. Photocatalytic performance evaluations

UV–visible light photocatalytic activities of the prepared samples were evaluated by degradation of the model organic pollutant of 2,4-DCP. The photocatalytic reactions were studied under a 500 W halogen lamp (Osram, Germany). A visible (Halogen, ECO OSRAM, 500W) lamp was used as the irradiation source, with an emission wavelength ranging from 350 to 800 nm with the predominant peak at 575 nm. The UV–visible light was focused on a 100 mL aqueous solution of 2,4-DCP (40 mg/L) and 50 mg of the photocatalyst. The suspension was magnetically stirred under darkness for 10 min before photocatalysis reaction, making sure that the adsorption/desorption of 2,4-DCP up to reach a stable equilibrium. Every interval time of 30 min, small aliquots (2 mL) were withdrawn and filtered to remove the photocatalyst particles and analyzed by Rayleigh UV-2601 UV/VIS spectrophotometer (λ_{max} = 227 nm).

3. Results and discussion

3.1. XRD analysis

The XRD pattern of the prepared TiO$_2$ is shown in Fig. 1(a). The peaks at 2θ = 27.4°, 36.1°, and 41.2° are indexed to the rutile phase of TiO$_2$ [47] while those at 2θ = 25.30°, 37.80°, 48.18°, and 54.09° are indexed to the anatase phase of TiO$_2$ (JCPDS 21-1272). The XRD analysis data confirmed that our prepared TiO$_2$ includes a low share of rutile phase but a high fraction of anatase phase. The XRD pattern of the prepared ternary Ag/AgCl/TiO$_2$ nanocomposite (Fig. 1(b)) showed the major diffractions of TiO$_2$ and some diffractions at about

2θ = 32.2°, 46.21°, 57.51°, and 67.4°, which can be indexed to the diffractions of AgCl (JCPDS no. 85-1355). The small peak at 2θ = 44.4° (Fig. 1(b)) can be assigned to the metallic silver, which makes the photocatalyst to be visible light responsive because of surface plasmonic resonance (SPR) effect of Ag nanoparticles [22]. Because of the low amount, high distribution, and small crystallite size of Ag particles, we did not detect the other diffractions of metallic Ag in XRD pattern of the ternary Ag/AgCl/TiO$_2$ nanocomposite (Fig. 1(b)) [22]. The XRD patterns of the prepared quaternary Ag/AgCl/TiO$_2$/MWCNTs nanocomposites are shown in Figs. 1(c)–(f). In XRD patterns of Ag/AgCl/TiO$_2$/MWCNTs nanocomposites (Figs. 1(c)–(f)), we did not observe MWCNTs peak at 2θ = 25.5° [48] since it was overlapped with the major diffraction of anatase TiO$_2$ at 2θ = 25.3°. Another explanation for not observing this diffraction might be the relatively large difference between the mass percentage of MWCNTs and TiO$_2$ and low crystallinity of MWCNTs [49]. The peaks at 2θ = 27.91°, 32.2°, 46.21°, 57.51°, and 67.4° can be attributed to the diffractions of AgCl (JCPDS no. 85-1355) in XRD patterns of quaternary nanocomposites, which also suggest that the AgCl particles are well crystallized. The presence of metallic Ag in the quaternary nanocomposite can be confirmed by the small diffraction at 2θ = 44.4° (Figs. 1(c)–(f)). The main diffraction of MWCNTs at 2θ = 25.5° did not observed in the XRD pattern of MWCNTs/TiO$_2$ (Fig. 1(g)), which was overlapped with the major diffraction of anatase TiO$_2$ at 2θ = 25.3° in this sample.

The average crystal size of TiO$_2$ at 2θ = 25.3° was calculated using Scherrer's equation [50].

$$D = K\lambda/\beta \cos\theta \tag{1}$$

where D is the average crystal size of the sample, λ the X-ray wavelength (1.54056 Å), β the full width at half maximum of the diffraction (radian), K is a coefficient (0.89), and θ is the diffraction angle at the peak maximum. The crystal size of TiO$_2$ in all the prepared nanocomposites is in the nanosize ranges from 8.78 to 12.85 nm (Table 2).

The lattice parameters ($a = b \neq c$) corresponding to tetragonal crystalline structure were obtained for (101) crystal plane of anatase phase (the major phase) using Eq. (2):

$$1/d^2 = (h^2 + k^2)/a^2 + l^2/c^2 \tag{2}$$

Considering the interplanar spacing (d_{hkl}), the distance between adjacent planes in the set (hkl), can be determined using the Bragg law:

$$d_{hkl} = \lambda/2 \sin\theta \tag{3}$$

The cell volume (tetragonal one) was calculated as:

$$V = a^2c \tag{4}$$

where a and c are the considered lattice parameters. Table 2 shows the lattice parameters of the prepared samples.

The obtained values of the lattice parameters for TiO$_2$ in the prepared samples match well with the anatase structure (Joint Committee for Powder Diffraction Standard, 78-2486) of TiO$_2$.
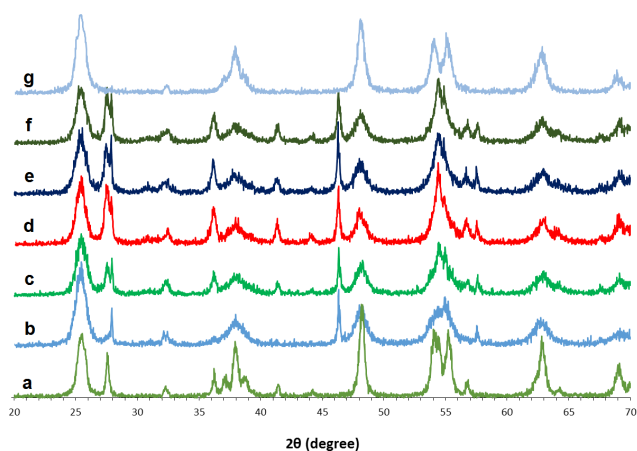

Fig. 1. The XRD patterns of (a) TiO$_2$, (b) Ag/AgCl/TiO$_2$, (c) Ag/AgCl/TiO$_2$/MWCNTs (2.00), (d) Ag/AgCl/TiO$_2$/MWCNTs (3.00), (e) Ag/AgCl/TiO$_2$/MWCNTs (4.00), (f) Ag/AgCl/TiO$_2$/MWCNTs (6.00), and (g) MWCNTs/TiO$_2$.

Table 2
Phase, crystal size, and lattice parameters of the prepared samples

Sample	Phase of TiO_2	Crystal size of TiO_2 (nm)	$a = b$ (Å)	c (Å)	$V = a^2c$ (Å³)
TiO_2	Anatase–Rutile	8.78	3.78	9.38	134.02
$MWCNTs/TiO_2$	Anatase–Rutile	12.85	3.80	9.81	141.65
$Ag/AgCl/TiO_2$	Anatase–Rutile	8.81	3.78	9.61	137.31
$Ag/AgCl/TiO_2/MWCNTs$ (2.00)	Anatase-Rutile	12.60	3.79	9.53	136.88
$Ag/AgCl/TiO_2/MWCNTs$ (3.00)	Anatase–Rutile	11.01	3.78	9.59	137.02
$Ag/AgCl/TiO_2/MWCNTs$ (4.00)	Anatase–Rutile	9.78	3.79	9.77	139.59
$Ag/AgCl/TiO_2/MWCNTs$ (6.00)	Anatase–Rutile	9.75	3.78	9.65	138.61

3.2. SEM/EDX and TEM analysis

Fig. 2 presents the SEM images of the prepared samples and Ag/AgCl nanoparticles loaded on the surface of TiO_2 and indicating the increase of the roughness of the TiO_2 surface. Here, Ag/AgCl has a porous morphology, which can expand the specific surface area and enhance the photocatalytic activity of the photocatalysts. To determine the chemical composition of the prepared nanocomposites (Fig. 3). The EDX analysis results (Fig. 3 and Table 3) prove the presence of C, Ti, Cl, and Ag atoms in the prepared samples. The absorption peak at 3 keV is for metallic silver nanocrystals and confirms the presence of nanocrystalline silver in the prepared samples [51]. The optical absorption peak at 2.8 keV, which is typical for the absorption of a chlorine atom, confirms the presence of chlorine in the samples containing AgCl [22]. The EDX result has verified that the obtained photocatalysts are composed of Ag and AgCl. Elemental mapping images of the prepared samples (Fig. 4) show that C, Ti, O, and Ag atoms are uniformly dispersed in the selected area of the samples.

Fig. 5 illustrates the TEM image of the best photocatalyst in this work (Ag/AgCl/TiO₂/MWCNTs(3)) nanocomposite at various magnifications. These images show that TiO_2 nanoparticles are uniformly dispersed on the wall of MWCNTs, and also demonstrate the loading of nanoparticles of Ag and AgCl on the TiO_2 nanoparticles and MWCNTs surface.

3.3. FTIR analysis

The FTIR spectra of the prepared samples are shown in Fig. 6. The vibration near 583 cm⁻¹ is indexed to the characterized vibrations of Ti–O in all the FTIR spectra. Ti–OH bond showed vibrations at ~3,400, 2,930, and 2,850 cm⁻¹ [52]. We detected the bending vibration of OH at ~1,630 cm⁻¹ for chemisorbed and/or physisorbed water molecules for all samples. There are stretching vibrations of Ti–O–Ti bond within the range of 700–500 cm⁻¹ [53]. The vibration at 1,515 cm⁻¹ is due to the C=C stretching, which is related to the structure of MWCNTs. It is clear from Fig. 6 that the vibrations at 500–700 and 1,515 cm⁻¹ are corresponding to TiO_2 and MWCNTs, respectively, suggesting that MWCNTs and TiO_2 nanoparticles are present in the prepared nanocomposites. In FTIR spectrum of $MWCNTs/TiO_2$ sample (Fig. 6(g)), the vibration at 1,393 cm⁻¹ confirms the interaction of COO⁻ groups on modified MWCNTs with the titanium dioxide. Here, the intense broadband in the vicinity of 550 cm⁻¹ can

be indexed to the combination of Ti–O–Ti and Ti–O–C vibrations between the MWCNTs and TiO_2 [54]. The extensive vibration ~3,250 cm⁻¹ can be assigned to the hydroxyl groups of TiO_2 and a hydrogen bond between TiO_2 surface and the carboxyl groups of MWCNTs. We did not detect the vibration at 1,385 cm⁻¹, assigned to the interaction between Ag and TiO_2 nanoparticles [55], probably due to the low amount of Ag.

3.4. DRS analysis

The UV–Vis DRS of the $Ag/AgCl/TiO_2$ and Ag/AgCl/TiO₂/MWCNTs photocatalysts showed strong absorption in the ultraviolet and visible-light regions (Fig. 7). The characteristic absorption peak of the AgCl and TiO_2 nanoparticles are within the UV region and the surface plasmon resonance of silver nanoparticles extended the absorption spectrum into the visible region [26,56,57]. Therefore, the ternary and quaternary nanocomposites are more efficient for photocatalytic degradation under visible light.

We calculated the band gap energy from the DR spectra according to Eq. (5) for the prepared samples.

$$E_{bg} = 1{,}240/\lambda \tag{5}$$

where E_{bg} is the band gap energy (eV) and λ is wavelength (nm) obtained from the DR spectra. The E_{bg} data of samples are summarized in Table 4. The results show that band gap energy of all the samples decreased slightly compared with pure TiO_2.

3.5. N_2 physisorption analysis

N_2 adsorption–desorption isotherms were prepared for all samples (Fig. 8). According to the IUPAC classification, the sorption isotherms for all of the prepared samples correspond to the type IV isotherm [58]. Textural and structural parameters of the obtained samples are shown in Table 5. Specific surface areas and average pore diameter were calculated according to the BET method. Moreover, pore volumes were derived from the desorption branch according to the BJH model. The BET surface area of $Ag/AgCl/TiO_2$ was ~82 m²/g, while that of Ag/AgCl/TiO₂/MWCNTs samples were around 72–84 m²/g, which is very similar to that of $Ag/AgCl/TiO_2$. N_2 adsorption and desorption results indicated that the introduction of MWCNTs had little effect on the structural properties on the $Ag/AgCl/TiO_2$.
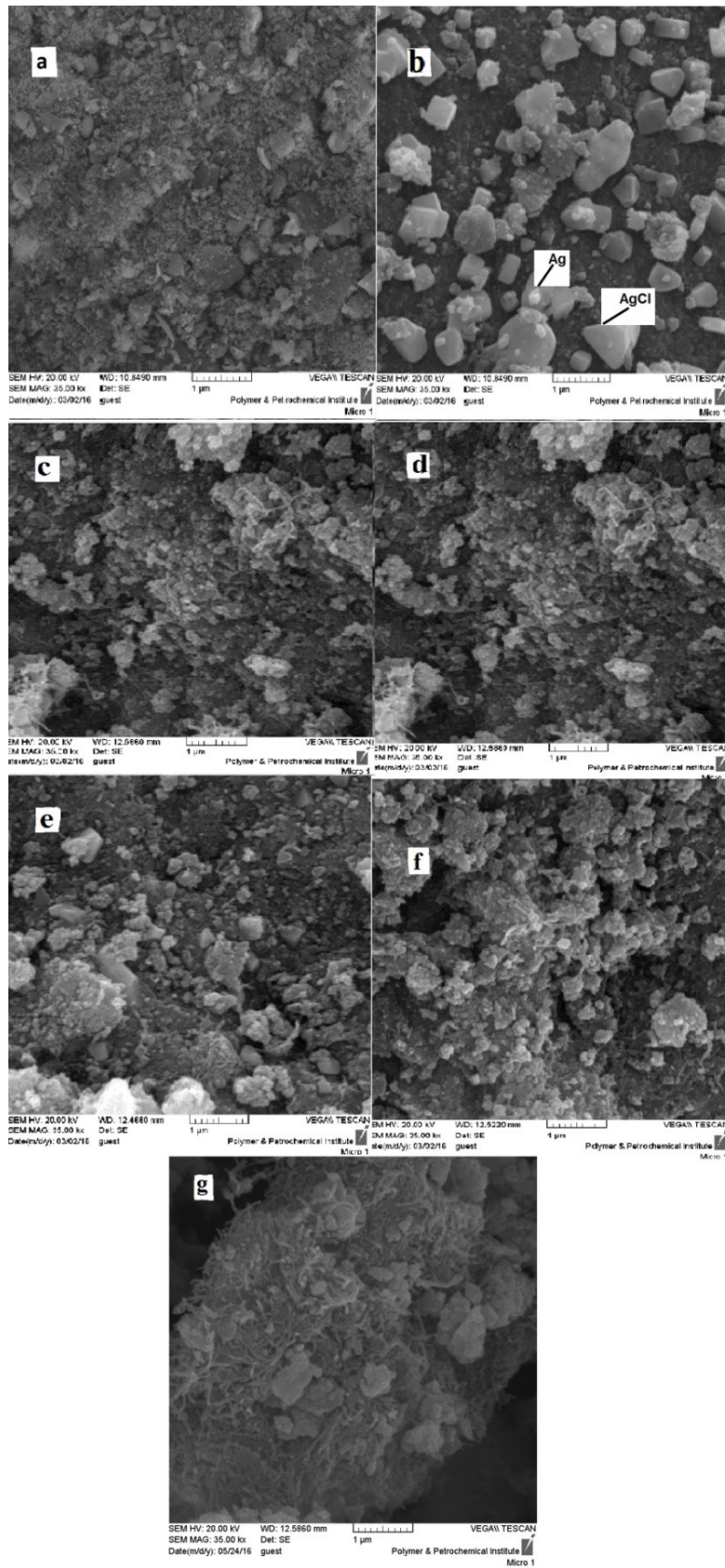
Fig. 2. SEM micrographs of (a) TiO_2, (b) $Ag/AgCl/TiO_2$, (c) $Ag/AgCl/TiO_2/MWCNTs$ (2.00), (d) $Ag/AgCl/TiO_2/MWCNTs$ (3.00), (e) $Ag/AgCl/TiO_2/MWCNTs$ (4.00), (f) $Ag/AgCl/TiO_2/MWCNTs$ (6.00), and (g) $MWCNTs/TiO_2$.
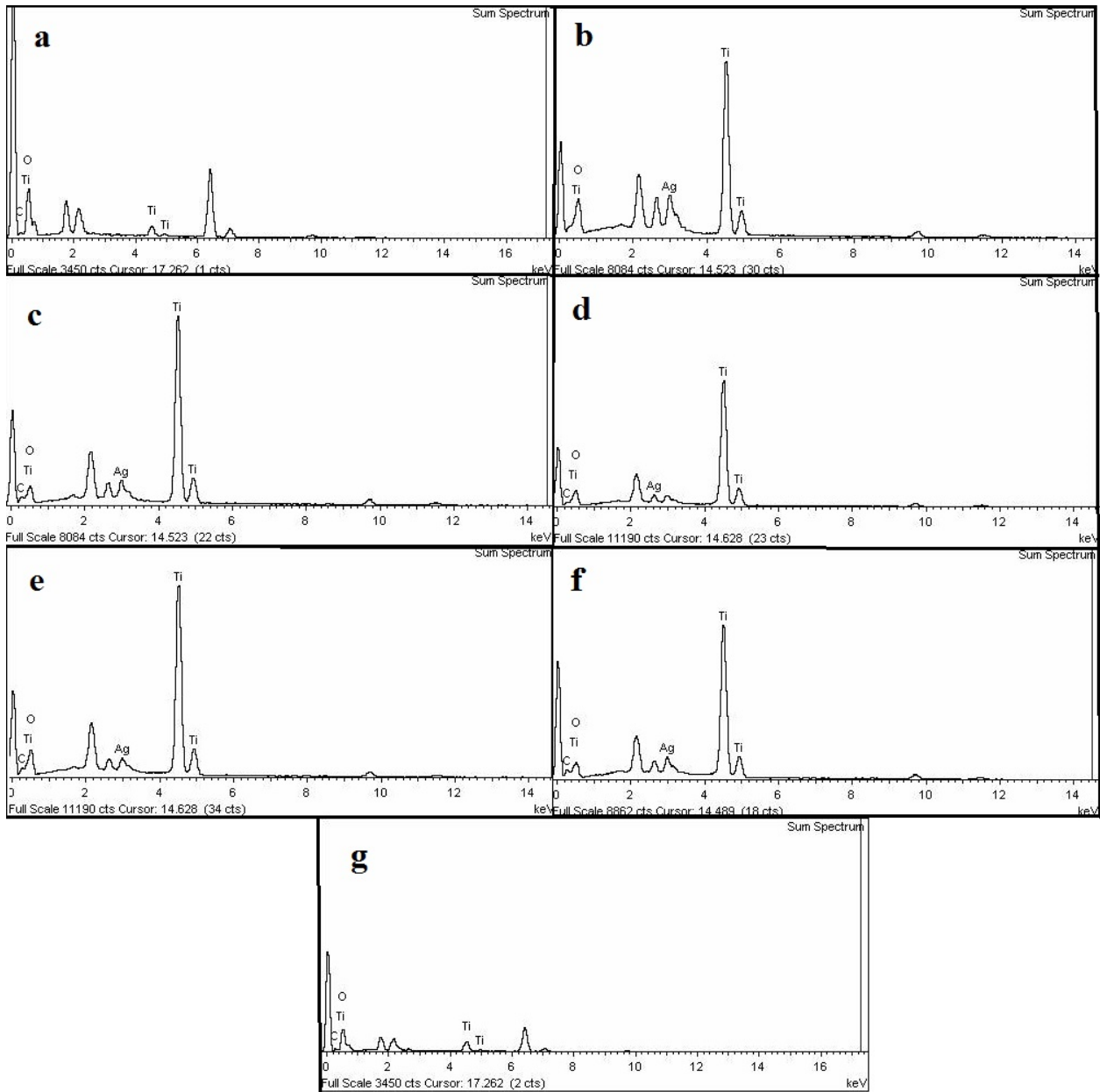
Fig. 3. EDX patterns of (a) TiO_2, (b) $Ag/AgCl/TiO_2$, (c) $Ag/AgCl/TiO_2/MWCNTs$ (2.00), (d) $Ag/AgCl/TiO_2/MWCNTs$ (3.00), (e) $Ag/AgCl/TiO_2/MWCNTs$ (4.00), (f) $Ag/AgCl/TiO_2/MWCNTs$ (6.00), and (g) $MWCNTs/TiO_2$.

Table 3
Elemental chemical analysis of the prepared samples

Sample	C (wt%)	Ti (wt%)	O (wt%)	Ag (wt%)	Cl (wt%)
TiO_2	8.42	54.09	37.80	–	–
$MWCNTs/TiO_2$	21.80	31.74	46.46	–	–
$Ag/AgCl/TiO_2$	5.49	36.39	52.01	6.11	3.40
$Ag/AgCl/TiO_2/MWCNTs$ (2.00)	10.38	44.00	38.81	6.80	4.65
$Ag/AgCl/TiO_2/MWCNTs$ (3.00)	10.59	41.45	43.88	4.08	2.35
$Ag/AgCl/TiO_2/MWCNTs$ (4.00)	11.06	39.88	44.87	4.19	2.65
$Ag/AgCl/TiO_2/MWCNTs$ (6.00)	13.84	40.64	38.89	6.63	4.20
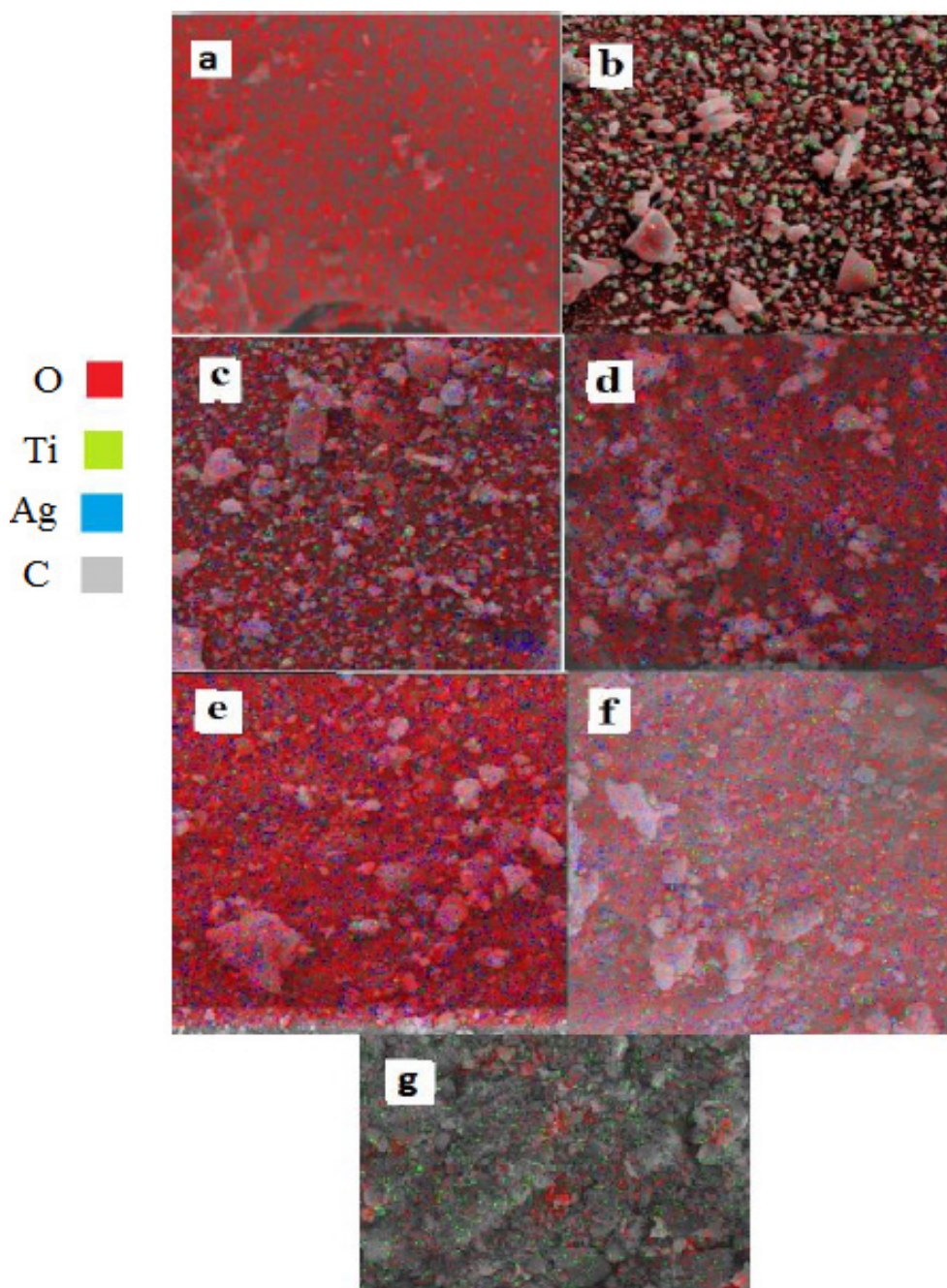
Fig. 4. Elemental mapping of (a) TiO_2, (b) Ag/AgCl/TiO_2, (c) Ag/AgCl/TiO_2/MWCNTs (2.00), (d) Ag/AgCl/TiO_2/MWCNTs (3.00), (e) Ag/AgCl/TiO_2/MWCNTs (4.00), and (f) Ag/AgCl/TiO_2/MWCNTs (6.00), and (g) TiO_2/MWCNTs.

3.6. Photocatalytic degradation of 2,4-DCP

The prepared Ag/AgCl/TiO_2/MWCNTs nanocomposites showed visible-light photocatalytic activity for degradation of 2,4-DCP (Fig. 9). The concentration of 2,4-DCP decreases steadily with increasing irradiation time and ~100% of the 2,4-DCP was degraded in 180 min, indicating that the prepared Ag/AgCl/TiO_2/MWCNTs nanocomposite has excellent photocatalytic performance under visible light. We gained 40% and about 57% degradations of 2,4-DCP in the presence of TiO_2 and Ag/AgCl/TiO_2, respectively, after 180 min under visible-light irradiation. The major photocatalytic efficiency of quaternary Ag/AgCl/TiO_2/MWCNTs nanocomposites can be explained according to the following aspects. First, the MWCNTs provide many adsorption sites, which are beneficial and enhance the photocatalytic efficiency of Ag/AgCl/TiO_2/MWCNTs nanocomposites. Thus, the adsorbed 2,4-DCP molecules can be transferred to the decomposition centers. Second, the surface plasmonic resonance effect of the Ag nanoparticles extends the absorption spectrum of the nanocomposites into the visible region and thus the photoinduced
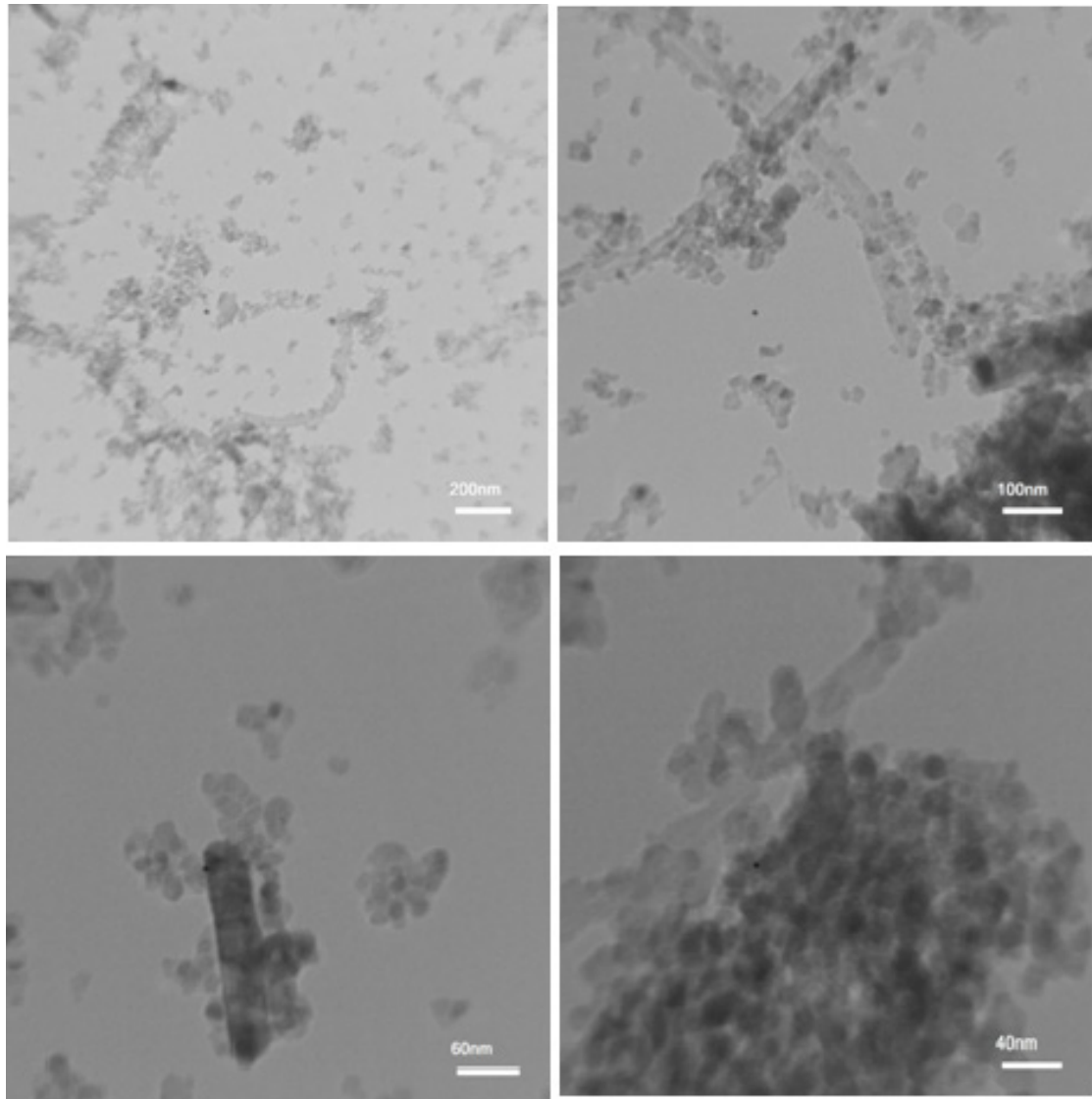
Fig. 5. TEM image of Ag/AgCl/TiO$_2$/MWCNTs (3.00) nanocomposite at various magnifications.
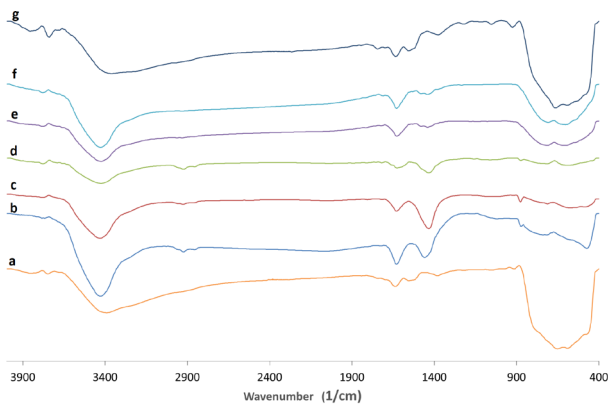

Fig. 6. FTIR spectra of (a) TiO$_2$, (b) Ag/AgCl/TiO$_2$, (c) Ag/AgCl/TiO$_2$/MWCNTs (2.00), (d) Ag/AgCl/TiO$_2$/MWCNTs (3.00), (e) Ag/AgCl/TiO$_2$/MWCNTs (4.00), (f) Ag/AgCl/TiO$_2$/MWCNTs (6.00), and (g) MWCNTs/TiO$_2$.
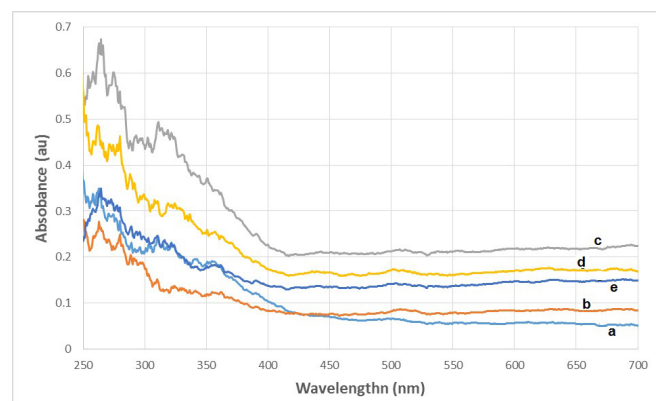

Fig. 7. DRS spectra of (a) Ag/AgCl/TiO$_2$, (b) Ag/AgCl/TiO$_2$/MWCNTs (2.00), (c) Ag/AgCl/TiO$_2$/MWCNTs (3.00), (d) Ag/AgCl/TiO$_2$/MWCNTs (4.00), and (e) Ag/AgCl/TiO$_2$/MWCNTs (6.00).

Table 4
The band gap energy of the prepared samples

Sample	Band gap energy (eV)
TiO_2	3.10
$Ag/AgCl/TiO_2$	2.75
$Ag/AgCl/TiO_2/MWCNTs$ (2.00)	2.48
$Ag/AgCl/TiO_2/MWCNTs$ (3.00	2.41
$Ag/AgCl/TiO_2/MWCNTs$ (4.00)	2.51
$Ag/AgCl/TiO_2/MWCNTs$ (6.00)	2.77

active species (such as h^+ and $O_2^{\bullet-}$) are generated through visible-light absorption. As discussed later, these active species could degrade 2,4-DCP target to the final carbon dioxide and some inorganic products. In other words, the high photocatalytic efficiency of $Ag/AgCl/TiO_2/MWCNTs$ nanocomposite could be assigned to the combined effect of the enhanced adsorption capacity and the surface plasmon resonance of Ag nanoparticles in the $Ag/AgCl/TiO_2/MWCNTs$ nanocomposite. The MWCNTs, acting as a photosensitizer, can trap the photoinduced electrons and form superoxide radical ion and/or hydroxyl radical on the surface of TiO_2, which are
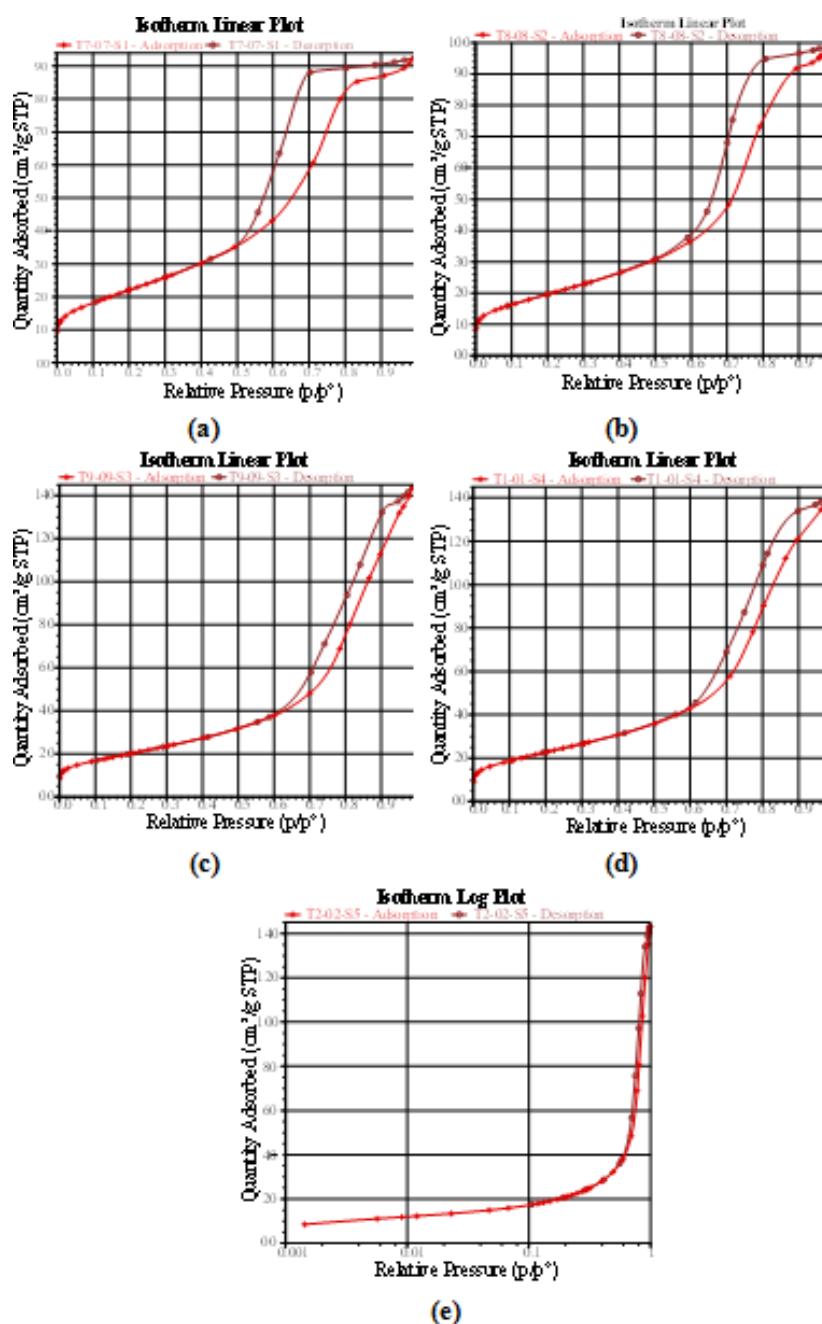

Fig. 8. N_2 adsorption–desorption isotherms for (a) $Ag/AgCl/TiO_2$, (b) $Ag/AgCl/TiO_2/MWCNTs$ (2.00), (c) $Ag/AgCl/TiO_2/MWCNTs$ (3.00), (d) $Ag/AgCl/TiO_2/MWCNTs$ (4.00), and (e) $Ag/AgCl/TiO_2/MWCNTs$ (6.00).

Table 5
Textural and structural parameters of the prepared sample

Sample	S_{BET} (m^2/g)	Average pore diameter (nm)	Pore volume (cm^3/g)
Ag/AgCl/TiO$_2$	81.930	6.920	0.145
Ag/AgCl/TiO$_2$/MWCNTs (2.00)	71.770	8.459	0.156
Ag/AgCl/TiO$_2$/MWCNTs (3.00)	74.204	11.510	0.224
Ag/AgCl/TiO$_2$/MWCNTs (4.00)	84.243	10.098	0.219
Ag/AgCl/TiO$_2$/MWCNTs (6.00)	77.045	11.162	0.223

Fig. 9. Photocatalytic degradation of 2,4-DCP over (a) TiO$_2$, (b) Ag/AgCl/TiO$_2$, (c) Ag/AgCl/TiO$_2$/MWCNTs (2.00), (d) Ag/AgCl/TiO$_2$/MWCNTs (3.00), (e) Ag/AgCl/TiO$_2$/MWCNTs (4.00), (f) Ag/AgCl/TiO$_2$/MWCNTs (6.00), and (g) MWCNTs/TiO$_2$ (2,4-DCP concentration 40 mg/L, 50 mg catalyst, 100 mL 2,4-DCP, visible light, irradiation time: 180 min).
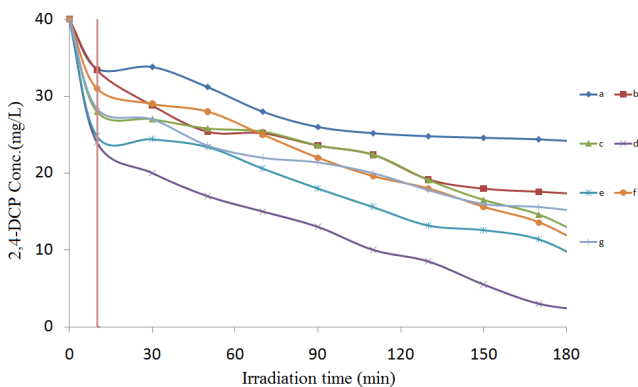

Fig. 10. Photocatalytic degradation of 2,4-DCP over (a) TiO$_2$, (b) Ag/AgCl/TiO$_2$, (c) Ag/AgCl/TiO$_2$/MWCNTs (2.00), (d) Ag/AgCl/TiO$_2$/MWCNTs (3.00), (e) Ag/AgCl/TiO$_2$/MWCNTs (4.00), (f) Ag/AgCl/TiO$_2$/MWCNTs (6.00), and (g) MWCNTs/TiO$_2$ (2,4-DCP concentration 40 mg/L, 50 mg catalyst, 100 mL 2,4-DCP, H$_2$O$_2$ concentration 0.01 M, visible light, irradiation time: 180 min).

responsible for the decomposition of the organic compound [49,59]. The MWCNTs increase the surface charge on TiO$_2$ in the hybrid photocatalysts. The surface charge may lead to modification of the fundamental process of electron/hole pair formation while applying visible light [60]. Accordingly, it may be the unique interaction between TiO$_2$ and the MWCNTs that provides the Ag/AgCl/TiO$_2$/MWCNTs nanocomposite with a higher photocatalytic efficiency in photocatalytic degradation of 2,4-DCP compare to pure TiO$_2$ and Ag/AgCl/TiO$_2$ samples. Among our prepared quaternary nanocomposites, Ag/AgCl/TiO$_2$/MWCNTs(3) showed the highest photocatalytic activity for decomposition of 2,4-DCP under visible light. These results confirm that the optimum mass ratio of MWCNTs and silver in nanocomposite is the prominent factor to produce Ag/AgCl/TiO$_2$/MWCNTs nanocomposite. The performance of the prepared nanocomposites for photocatalytic degradation of 2,4-DCP may be improved even more by addition of hydrogen peroxide as an oxidant to the photocatalytic reactor (Fig. 10). In the absence of H$_2$O$_2$, ~90% of 2,4-DCP is eliminated within 180 min in the presence of Ag/AgCl/TiO$_2$/MWCNTs(3). In the presence of H$_2$O$_2$, we obtained ~100% degradation for 2,4-DCP because more hydroxyl radicals are produced compared with the conditions without using H$_2$O$_2$. Hydroxyl radicals can be generated through the direct photolysis of H$_2$O$_2$ [61,62] or by the reaction of hydrogen peroxide with superoxide radical [63,64]. However, in the present work, the visible-light source cannot perform direct photolysis of H$_2$O$_2$ because the wavelengths shorter than 300 nm is needed for photocleavage of
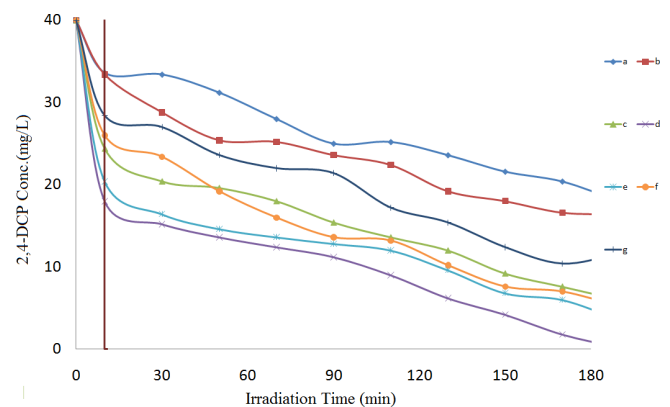
the H$_2$O$_2$ molecules. Generation of hydroxyl radicals in our photocatalytic reactor can be explained according to the below reaction:

$$H_2O_2 + O_2^{\bullet-} \rightarrow OH^{\bullet} + OH^- + O_2 \qquad (6)$$

We can obtain a higher decomposition rate for 2,4-DCP degradation in the presence of more hydroxyl radicals. This photocatalyst did not show any photocatalytic activity under darkness, suggesting that it is necessary to photoexcite both TiO$_2$ and the silver and enhance the photocatalytic efficiency of the prepared nanocomposite. The stability of the photocatalyst is very important for its practical and environmental application. Hence, the stability of plasmonic photocatalyst Ag/AgCl/TiO$_2$/MWCNTs nanocomposite was further investigated by the recycle experiments of the photocatalyst. After four cycles, the photocatalytic activity of the best photocatalyst (Ag/AgCl/TiO$_2$/MWCNTs(3)) does not exhibit any significant loss of activity (not shown here), indicating that this sample has a good stability during the photocatalytic degradation of 2,4-DCP.

3.7. Photocatalytic degradation mechanism

The photocatalytic activity of the Ag/AgCl/TiO$_2$/MWCNTs nanocomposite can be explained by the following proposed mechanism, which is similar to the one proposed for plasmonic photocatalysis (Fig. 11) [65,66]:
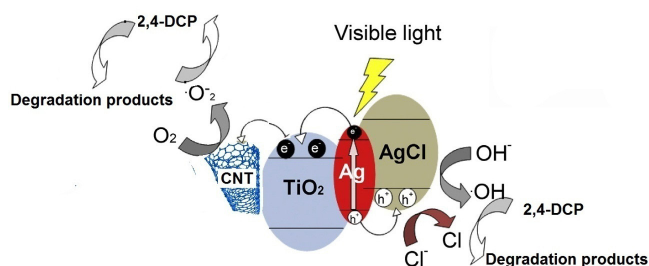
Fig. 11. Our proposed mechanism for 2,4-DCP degradation by quaternary Ag/AgCl/TiO$_2$/MWCNTs nanocomposite under visible light.

Photogenerated electron–hole pairs are formed due to surface plasmon resonance in silver nanoparticles after visible-light absorption. These electrons are transferred from the silver nanoparticles into the conduction band of the TiO$_2$ semiconductor. The Fermi level of TiO$_2$ and silver nanoparticles is the same. TiO$_2$ cannot be excited by visible light and its Fermi level keeps unchanged. On the other hand, Ag nanoparticles can absorb visible light due to its SPR absorption, which results in the upshift of Fermi level of Ag nanoparticles. Therefore, the photoexcited electrons at the silver nanoparticles can be easily transferred into the conduction band of the TiO$_2$ semiconductor. The injected electrons can be transferred to the adsorbed O$_2$. In this process, first, some active species such as superoxide radical O$_2^{\bullet-}$ anions are generated then followed by the protonation of the produced HOO$^\bullet$ radicals. The HOO$^\bullet$ radicals and the trapped electrons react together and produce H$_2$O$_2$ and then $^\bullet$OH radicals formed [67]. These $^\bullet$OH active species attack the 2,4-DCP and decomposition and thus mineralization of 2,4-DCP can take place. Nevertheless, the left holes can be transferred to the AgCl surface due to the negative surface charge [65], which could cause the oxidation of Cl$^-$ ions to Cl^0 atoms [66,68–71]. Because of the high oxidation ability of the chlorine atoms, the 2,4-DCP could be oxidized by the chlorine atoms and hence the Cl^0 could be reduced to chloride ions again. Therefore, the Ag/AgCl/TiO$_2$/MWCNTs nanocomposite could remain stable without deterioration [66,70,71]. In the presence of MWCNTs, the effective separation of the photogenerated electron/hole that generates in silver nanoparticles under visible light can be improved while its recombination is suppressed since MWCNTs can store a large number of electrons and transport these. Therefore, the photocatalytic activity of Ag/AgCl/TiO$_2$/MWCNTs nanocomposite was improved because of the effective separation of the photogenerated electron/hole as well as the adsorption and photocatalysis properties of the four components of the nanocomposite.

4. Conclusion

In summary, visible-light-driven quaternary Ag/AgCl/TiO$_2$/MWCNTs photocatalysts containing different amounts of MWCNTs were prepared through the simple sol–gel method. The prepared photocatalysts were characterized by different analysis techniques such as XRD, DRS, FTIR, TEM, BET, and SEM/EDX. The prepared samples exhibited a high adsorption capacity and an excellent visible-light photocatalytic activity for 2,4-DCP degradation as a model of organic pollutants. The high photocatalytic activity can be attributed to both the high specific surface areas of the MWCNTs and the plasmon resonance of silver nanoparticles. As a result, the high adsorption capacity and efficient photocatalytic performance of the prepared quaternary Ag/AgCl/TiO$_2$/MWCNTs nanocomposites make them suitable choices for environmental applications.

Acknowledgement

References

[1] J. Low, B. Cheng, J. Yu, Surface modification and enhanced photocatalytic CO^2 reduction performance of TiO$_2$: a review, Appl. Surf. Sci., 392 (2017) 658–686.

[2] D. Tang, G. Zhang, Ultrasonic-assistant fabrication of cocoon-like Ag/AgFeO$_2$ nanocatalyst with excellent plasmon enhanced visible-light photocatalytic activity, Ultrason. Sonochem., 37 (2017) 208–215.

[3] S. Girish Kumar, K.S.R. Koteswara Rao, Comparison of modification strategies towards enhanced charge carrier separation and photocatalytic degradation activity of metal oxide semiconductors (TiO$_2$, WO$_3$ and ZnO), Appl. Surf. Sci., 391 (2017) 124–148.

[4] L.V. Bora, R.K. Mewada, Visible/solar light active photocatalysts for organic effluent treatment: fundamentals, mechanisms and parametric review, Renew. Sustain. Energy Rev., 76 (2017) 1393–1421.

[5] H. Gan, G. Zhang, H. Huang, Enhanced visible-light-driven photocatalytic inactivation of *Escherichia coli* by Bi$_2$O$_2$CO$_3$/Bi$_3$NbO$_7$ composites, J. Hazard. Mater., 250–251 (2013) 131–137.

[6] Z. Wan, G. Zhang, X. Wu, S. Yin, Novel visible-light-driven Z-scheme Bi$_{12}$GeO$_{20}$/g-C$_3$N$_4$ photocatalyst: oxygen-induced pathway of organic pollutants degradation and proton assisted electron transfer mechanism of Cr(VI) reduction, Appl. Catal., B, 207 (2017) 17–26.

[7] O. Diwald, T.L. Thompson, T. Zubkov, E.G. Goralski, S.D. Walck, J.T. Yates, Photochemical activity of nitrogen-doped rutile TiO$_2$(110) in visible light, J. Phys. Chem. B, 108 (2004) 6004–6008.

[8] J.X. Li, J.H. Xu, W.L. Dai, K.N. Fan, Dependence of Ag deposition methods on the photocatalytic activity and surface state of TiO$_2$ with twist like helix structure, J. Phys. Chem. C, 113 (2009) 8343–8349.

[9] H.M. Sung-Suh, J.R. Choi, H.J. Hah, S.M. Koo, Y.C. Bae, Comparison of Ag deposition effects on the photocatalytic activity of nanoparticulate TiO$_2$ under visible and UV light irradiation, J. Photochem. Photobiol., A, 163 (2004) 37–44.

[10] J.G. Yu, J.F. Xiong, B. Cheng, S.W. Liu, Fabrication and characterization of Ag–TiO$_2$ multiphase nanocomposite thin films with enhanced photocatalytic activity, Appl. Catal., B, 60 (2005) 211–221.

[11] K. Awazu, M. Fujimaki, C. Rockstuhl, J. Tominaga, H. Murakami, Y. Ohki, N. Yoshida, T. Watanabe, A plasmonic photocatalyst consisting of silver nanoparticles embedded in titanium dioxide, J. Am. Chem. Soc., 130 (2008) 1676–1680.

[12] A. Ayati, A. Ahmadpour, F.F. Bamoharram, B. Tanhaei, M. Manttari, M. Sillanpaa, A review on catalytic applications of Au/TiO$_2$ nanoparticles in the removal of water pollutant, Chemosphere, 107 (2014) 163–174.

[13] L. Gomathi Devi, R. Kavitha, A review on plasmonic metal/TiO$_2$ composite for generation, trapping, storing and dynamic vectorial transfer of photogenerated electrons across the Schottky junction in a photocatalytic system, *Appl. Surf. Sci.*, 360 (2016) 601–622.

[14] W. Liu, D. Chen, S.H. Yoo, S.O. Cho, Hierarchical visible light-response Ag/AgCl@TiO$_2$ plasmonic photocatalysts for organic dye degradation, Nanotechnology, 24 (2013) 405706–405712.

[15] B. Cai, J. Wang, S. Gan, D. Han, Z. Wu, L. Niu, A distinctive red Ag/AgCl photocatalyst with efficient photocatalytic oxidative and reductive activities, J. Mater. Chem. A, 2 (2014) 5280–5286.

[16] W. Liao, Y. Zhang, M. Zhang, M. Murugananthan, S. Yoshihara, Photoelectrocatalytic degradation of microcystin-LR using Ag/AgCl/TiO$_2$ nanotube arrays electrode under visible light irradiation, Chem. Eng. J., 231 (2013) 455–463.

[17] L. Qi, J. Yu, G. Liu, P.K. Wong, Synthesis and photocatalytic activity of plasmonic Ag@AgCl composite immobilized on titanate nanowire films, Catal. Today, 224 (2014) 193–199.

[18] D. Wang, Y. Li, G.L. Puma, C. Wang, P. Wang, W. Zhang, Q. Wang, Ag/AgCl@helical chiral TiO$_2$ nanofibers as a visible-light driven plasmon photocatalyst, Chem. Commun., 49 (2013) 10367–10369.

[19] J. Guo, B. Ma, A. Yin, K. Fan, W. Dai, Highly stable and efficient Ag/AgCl@TiO$_2$ photocatalyst: preparation, characterization, and application in the treatment of aqueous hazardous pollutants, J. Hazard. Mater., 211–212 (2012) 77–82.

[20] X.L. Wang, H.Y. Yin, Q.L. Nie, W.W. Wu, Y. Zhang, Q.L. Yuan, Hierarchical Ag/AgCl-TiO$_2$ hollow spheres with enhanced visible-light photocatalytic activity, Mater. Chem. Phys., 185 (2017) 143–151.

[21] Y. Yang, R. Liu, G. Zhang, L. Gao, W. Zhang, Preparation and photocatalytic properties of visible light driven Ag-AgCl-TiO$_2$/palygorskite composite, J. Alloys Compd., 657 (2016) 801–808.

[22] L. Yinghua, W. Huan, L. Li, C. Wenquan, Facile synthesis of Ag@AgCl plasmonic photocatalyst and its photocatalytic degradation under visible light, Rare Met. Mater. Eng., 44 (2015) 1088–1093.

[23] S. Liu, J. Zhu, Q. Yang, P. Xu, J. Ge, X. Guo, Synthesis and characterization of cube-like Ag@AgCl-doped TiO$_2$/fly ash cenospheres with enhanced visible-light photocatalytic activity, Opt. Mater., 53 (2016) 73–79.

[24] H. Yin, X. Wang, L. Wang, Q.-L. Nie, Y. Zhang, Q. Yuan, W. Wu, Ag/AgCl modified self-doped TiO$_2$ hollow sphere with enhanced visible light photocatalytic activity, J. Alloys Compd., 657 (2016) 44–52.

[25] Z. Zhao, Y. Wang, J. Xu, C. Shang, Y. Wang, AgCl-loaded mesoporous anatase TiO$_2$ with large specific surface area for enhancing photocatalysis, Appl. Surf. Sci., 351 (2015) 416–424.

[26] J. Zhou, Y. Cheng, J. Yu, Preparation and characterization of visible-light-driven plasmonic photocatalyst Ag/AgCl/TiO$_2$ nanocomposite thin films, J. Photochem. Photobiol., A, 223 (2011) 82–87.

[27] D. Wu, L. Wang, X. Song, Y. Tan, Enhancing the visible-light-induced photocatalytic activity of the self-cleaning TiO$_2$-coated cotton by loading Ag/AgCl nanoparticles, Thin Solid Films, 540 (2013) 36–40.

[28] J. Cao, B. Xu, B. Luo, H. Lin, S. Chen, Preparation, characterization and visible-light photocatalytic activity of AgI/AgCl/TiO$_2$, Appl. Surf. Sci., 257 (2011) 7083–7089.

[29] P. Zhou, J. Yu, M. Jaroniec, All-solid-state Z-scheme photocatalytic systems, Adv. Mater., 26 (2014) 4920–4935.

[30] Y. Li, Y. Ding, Porous AgCl/Ag nanocomposites with enhanced visible lightphotocatalytic properties, J. Phys. Chem. C, 114 (2010) 3175–3317.

[31] J. Tian, R. Liu, G. Wang, Y. Xu, X. Wang, H. Yu, Dependence of metallic Ag on the photocatalytic activity and photoinduced stability of Ag/AgCl photocatalyst, Appl. Surf. Sci., 319 (2014) 324–331.

[32] S.X. Liu, X.Y. Chen, X. Chen, A TiO$_2$/AC composite photocatalyst with high activity and easy separation prepared by a hydrothermal method, J. Hazard. Mater., 143 (2007) 257–263.

[33] P. Singh, M.C. Vishnu, K.K. Sharma, R. Singh, S. Madhav, D. Tiwary, Comparative study of dye degradation using TiO$_2$-activated carbon nanocomposites as catalysts in photocatalytic, sonocatalytic, and photosonocatalytic reactor, Desal. Wat. Treat., 57 (2016) 20552–20564.

[34] L.W. Zhang, H.B. Fu, Y.F. Zhu, Efficient TiO$_2$ photocatalysts from surface hybridization of TiO$_2$ particles with graphite-like carbon, Adv. Funct. Mater., 18 (2008) 2180–2189.

[35] N.R. Khalid, A. Majid, M. Bilal Tahir, N.A. Niaz, S. Khalid, Carbonaceous-TiO$_2$ nanomaterials for photocatalytic degradation of pollutants: a review, Ceram. Int., 43 (2017) 14552–14571.

[36] S.L. Cha, K.T. Kim, K.H. Lee, C.B. Mo, Y.J. Jeng, S.H. Hong, Mechanical and electrical properties of cross-linked carbon nanotubes, Carbon, 46 (2008) 482–488.

[37] P. Serp, M. Corrias, P. Kalck, Carbon nanotubes and nanofibers in catalysis, Appl. Catal., A, 253 (2003) 337–358.

[38] W. Wang, P. Serp, P. Kalck, J.L. Faria, Photocatalytic degradation of phenol on MWNT and titania composite catalysts prepared by a modified sol–gel method, Appl. Catal., B, 56 (2005) 305–312.

[39] F. Shahrezaei, P. Pakraven, A. Hemati Azandaryani, M. Pirsaheb, A.M. Mansouri, Preparation of multi-walled carbon nanotube-doped TiO$_2$ composite and its application in petroleum refinery wastewater treatment, Desal. Wat. Treat., 57 (2016) 14443–14452.

[40] T.Y. Lee, P.S. Alegaonkar, J.B. Yoo, Fabrication of dye sensitized solar cell using TiO$_2$ coated carbon nanotube, Thin Solid Films, 515 (2007) 5131–5135.

[41] Y. Yao, G. Li, S. Ciston, R.M. Lueptow, K.A. Gray, Photoreactive TiO$_2$/carbon nanotube composites: synthesis and reactivity, Environ. Sci. Technol., 42 (2008) 4952–4957.

[42] J. Michałowicz, W. Duda, Phenols – sources and toxicity, Pol. J. Environ. Stud., 16 (2007) 347–362.

[43] H.C. Lee, J.H. In, J.H. Kim, K.Y. Hwang, C.H. Lee, Kinetic analysis for decomposition of 2,4-dichlorophenol by supercritical water oxidation, Korean J. Chem. Eng., 22 (2005) 882–888.

[44] M.M. Ba Abbad, A.A.H. Kadhum, A.A. Al Amiery, A.B. Abu Bakar Mohamad, M.S. Takriff, Toxicity evaluation for low concentration of chlorophenols under solar radiation using zinc oxide (ZnO) nanoparticles, Int. J. Phys. Sci., 7 (2012) 48–52.

[45] K. Arnoldsson, P.L. Andersson, P. Haglund, Formation of environmentally relevant brominated dioxins from 2,4,6,-tribromophenol via bromoperoxidase-catalyzed dimerization, Environ. Sci. Technol., 46 (2012) 7239–7244.

[46] J. Bandara, J.A. Mielczarski, A. Lopez, J. Kiwi, Sensitized degradation of chlorophenols on Iron oxides induced by visible light: comparison with titanium oxide, Appl. Catal., B, 34 (2001) 321–333.

[47] K.V. Baiju, P. Shajesh, W. Wunderlich, Effect of tantalum addition on anatase phase stability and photoactivity of aqueous sol–gel derived mesoporous titania, J. Mol. Catal. A, 276 (2007) 41–46.

[48] B. Ahmmad, Y. Kusumoto, S. Somekawa, M. Ikeda, Carbon nanotubes synergistically enhance photocatalytic activity of TiO$_2$, Catal. Commun., 9 (2008) 1410–1413.

[49] W. Wang, P. Serp, P. Kalck, Visible light photodegradation of phenol on MWNT-TiO$_2$ composite catalysts prepared by a modified sol–gel method, J. Mol. Catal. A: Chem., 235 (2005) 194–199.

[50] M. Khan, W. Cao, Cationic (V, Y)-codoped TiO$_2$ with enhanced visible light induced photocatalytic activity: a combined experimental, theoretical study, J. Appl. Phys., 114 (2013) 183514.

[51] S. Kaviya, J. Santhanalakshmi, B. Viswanathan, J. Muthumar, K. Srinivasan, Biosynthesis of silver nanoparticles using citrus sinensis peel extract and its antibacterial activity, Spectrochim. Acta, 79 (2011) 594–598.

[52] Y. Wang, Y. Huang, W. Ho, Biomolecule-controlled hydrothermal synthesis of C–N–S-tridoped TiO$_2$ nanocrystalline photocatalysts for NO removal under simulated solar light irradiation, J. Hazard. Mater., 169 (2009) 77–87.

[53] E. Bae, W. Choi, Highly enhanced photoreductive degradation of perchlorinated compounds on dye-sensitized metal/TiO$_2$ under visible light, Environ. Sci. Technol., 37 (2003) 147–152.

[54] G. Hu, X. Meng, X. Feng, Y. Ding, S. Zhang, M. Yang, Anatase TiO$_2$ nanoparticles/carbon nanotubes nanofibers: preparation, characterization and photocatalytic properties, J. Mater. Sci., 42 (2007) 7162–7170.

[55] J. Garcia-Serrano, E. Gomez-Hernandez, M. Ocampo-Fernandez, U. Pal, Effect of Ag doping on the crystallization and phase transition of TiO$_2$ nanoparticles, Curr. Appl. Phys., 9 (2009) 1097–1105.

[56] P. Wang, B.B. Huang, Z.Z. Lou, X.Y. Zhang, X.Y. Qin, Y. Dai, Z.K. Zheng, X.N. Wang, Synthesis of highly efficient Ag@AgCl plasmonic photocatalysts with various structures, Chem. A Eur. J., 16 (2010) 538–544.

[57] C. An, S. Peng, Y. Sun, Facile synthesis of sunlight-driven AgCl:Ag plasmonic nanophotocatalyst, Adv. Mater., 22 (2010) 2570–2574.

[58] M. Thommes, Physical adsorption characterization of nanoporous materials, Chem. Ing. Tech., 82 (2010) 1059–1073.

[59] Y. Yu, J.C. Yu, J.G. Yu, Y.C. Kwok, Y.K. Che, J.C. Zhao, L. Ding, W.K. Ge, P.K. Wong, Enhancement of photocatalytic activity of mesoporous TiO_2 by using carbon nanotubes, Appl. Catal., A, 289 (2005) 186–196.

[60] J. Sun, M. Iwasa, L. Gao, Q.H. Zhang, Single-walled carbon nanotubes coated with titania nanoparticles, Carbon, 42 (2004) 895–899.

[61] A. Ebrahimian, M.A. Zanjanchi, Heterogeneous photocatalytic degradation of 4-chlorophenol by immobilization of cobalt tetrasulphophthalocyanine onto MCM-41, Korean J. Chem. Eng., 31 (2014) 218–223.

[62] A. Ebrahimian, M.A. Zanjanchi, H. Noei, M. Arvand, Y. Wang, TiO_2 nanoparticles containing sulphonated cobalt phthalocyanine: preparation, characterization and photocatalytic performance, J. Environ. Chem. Eng., 2 (2014) 484–494.

[63] A. Ebrahimian, M.A. Zanjanchi, M. Arvand, Sulphonated cobalt phthalocyanine–MCM-41: an active photocatalyst for degradation of 2,4-dichlorophenol, J. Hazard. Mater., 175 (2010) 992–100.

[64] B.J.P.A. Cornish, L.A. Lawton, P.K.J. Robertson, Hydrogen peroxide enhanced photocatalytic oxidation of microcystin-LR using titanium dioxide, Appl. Catal., B, 25 (2000) 59–67.

[65] Q.J. Xiang, J.G. Yu, B. Cheng, H.C. Ong, Microwave-hydrothermal preparation and visible-light photoactivity of plasmonic photocatalyst Ag-TiO_2 nanocomposite hollow spheres, Chem. Asian J., 5 (2010) 1466–1474.

[66] J.G. Yu, G.P. Dai, B.B. Huang, Fabrication and characterization of visible-light-driven plasmonic photocatalyst Ag/AgCl/TiO_2 nanotube arrays, J. Phys. Chem. C, 113 (2009) 16394–16401.

[67] P.V. Laxma Reddy, B. Kavitha, P.A. Kumar Reddy, K.-H. Kim, TiO_2-based photocatalytic disinfection of microbes in aqueous media: a review, Environ. Res., 154 (2017) 296–303.

[68] G. Begum, J. Manna, R.K. Rana, Controlled orientation in a bio-inspired assembly of Ag/AgCl/ZnO nanostructures enables enhancement in visible-light-induced photocatalytic performance, Chem. A Eur. J., 18 (2012) 6847–6853.

[69] X. Jia, Y. Liu, J. Sun, H. Sun, Z. Su, X. Pan, R. Wang, Theoretical investigation of the reactions of $CF_3CHFOCF_3$ with the OH radical and Cl atom, J. Phys. Chem. A, 114 (2009) 417–424.

[70] P. Wang, B.B. Huang, X.Y. Qin, X.Y. Zhang, Y. Dai, J.Y. Wei, M.H. Whangbo, Ag@AgCl: a highly efficient and stable photocatalyst active under visible light, Angew. Chem. Int. Ed., 47 (2008) 7931–7933.

[71] H. Xu, H.M. Li, J. Xia, S. Yin, Z. Luo, L. Liu, L. Xu, One-pot synthesis of visible-light-driven plasmonic photocatalyst Ag/AgCl in ionic liquid, ACS Appl. Mater. Interfaces, 3 (2011) 22–29.